International Journal of Nanomedicine

Dovepress
open access to scientific and medical research

Open Access Full Text Article

ORIGINAL RESEARCH

The Fabrication and Function of Strontium-modified Hierarchical Micro/Nano Titanium Implant

This article was published in the following Dove Press journal:
International Journal of Nanomedicine

Haiyan Wang[1]
Qiuping Xu[1]
Hui Hu[2]
Chunling Shi[3]
Ziyan Lin[3]
Huixi Jiang[3]
Huaipu Dong[3]
Jing Guo[1]

[1]Department of Orthodontics, School and Hospital of Stomatology, Cheeloo College of Medicine, Shandong University & Shandong Key Laboratory of Oral Tissue Regeneration & Shandong Engineering Laboratory for Dental Materials and Oral Tissue Regeneration, Jinan, Shandong, 250012, People's Republic of China; [2]Osaka Dental University Kusuha School, Hirakata City, Osaka 573-1121, Japan; [3]School and Hospital of Stomatology, Wenzhou Medical University, Wenzhou, 325027, People's Republic of China

Video abstract

Point your SmartPhone at the code above. If you have a QR code reader the video abstract will appear. Or use: https://youtu.be/-6Wh1M0igI0

Correspondence: Jing Guo
Department of Orthodontics, Room 201, School and Hospital of Stomatology, Shandong University, 44-1 Wenhua West Road, Jinan, Shandong 250012, Mainland China
Email guojing@sdu.edu.cn

Background: Relying on surface topography alone to enhance the osteointegration of implants is still inadequate. An effective way to combine long-term ion release and surface topography to enhance osteogenic property is urgently needed.

Purpose: The objective of this study is to fabricate a long-term strontium ion release implant system and confirm the biological function in vitro and in vivo.

Methods: The biomimic surface was fabricated through alkali-heat treatment and magnetron sputtering. The in vitro biological function assays were determined by MTT, fluorescence staining, alkaline phosphatase activity, extracellular mineralization, and quantitative real-time polymerase chain reaction assays. The in vivo experiments were detected by micro-CT, HE staining and Masson staining.

Results: The biomimic surface structure has been successfully fabricated. The in vitro cell assays determined that AH-Ti/Sr90 possessed the best biological function. The in vivo experiments demonstrated that AH-Ti/Sr90 could promote osteointegration significantly under both in normal and osteoporotic conditions.

Conclusion: We determined that AH-Ti/Sr90 possesses the best osteogenic property, long-term ion release capacity and osteointegration promotion ability. It has potential clinic application prospects.

Keywords: titanium, alkali-heat treatment, magnetron sputtering, osteogenic differentiation, osteoclast inhibition

Introduction

Titanium implants and its alloys are still the mainstream materials adopted in biomedical area, especially dental implantology.[1] However, there are still some disadvantages such as inert surfaces, potential allergic reaction, and the lack of osteogenic induction, impeding the success of implant surgery.[2] What is more, osteoporosis, commonly seen in postmenopausal women would alter the bone microstructure and decrease the bone volume and bone density simultaneously.[3] Therefore, numerous methods are highly warranted to endow the implant with osteogenic property and anti-osteoclast ability. Though various physical and chemical methods have been used to modify the titanium surface, the osteointegration of bone-to-implant has not reached an ideal level.[4–6] Some techniques like sandblasting-acid etching, anodization, and calcium phosphate coating have been applied in clinical implant production and even became the mainstream implants in oral implantology like SLA-active of NOBEL company.[7] In addition, the coating methods like magnetron sputtering, atomic layer deposition, chemical vapor deposition (CVD), physical vapor deposition (PVD) have potential clinical

applications which can endow the titanium surfaces with multiple functions and thus enhance the osteointegration.[8–10]

According to previous studies, both the surface topography and the ion function can enhance the osteogenic property of osteoblast cells and thus increase the osteointegration.[11–16] From a biomimic point of view, micro/nanostructure, which simulate trabecular bone structure is conducive to bone regeneration.[12] In addition, the metal ions (tantalum, strontium, zinc, etc) have also been confirmed to significantly promote osteogenesis.[17–19] Reports have confirmed that titanium with alkali-heat treatment can increase osteoblast cell adhesion, cell elongation and cell proliferation, but relying only on structure alone to enhance osteoblast osteogenic induction is still inadequate.[20] Therefore, the combination of surface topography and ion function aroused the clinic's interest tremendously.

Strontium (Sr), a necessary element for bone formation in the human body, has been confirmed conducive to bone formation.[21–23] The reason is attributed to the two-way regulated function, which can enhance osteoblast differentiation and compromise osteoclast activity simultaneously.[23] In addition, strontium can enhance the activity of MSC originated from both normal and osteoporosis ones, which further indicates that strontium has superior promotion to the bone formation in normal and osteoporotic bodies.[22–24] Because of the function of strontium, Bianchi et al had doped strontium into calcium phosphate coatings on PEEK. However, the ion release is not able to achieve long-term release.[24] Therefore, a better ion release system needs to be fabricated and a suitable coating needs to be explored.

Above all, an effective method to utilize the metal ion function and to generate long-term release is needed. In this work, we coated $SrTiO_3$ nanolayer on alkali-heat treated titanium (AH-Ti) by magnetron sputtering and different durations of magnetron sputtering were performed to select the best duration of magnetron sputtering. We hypothesize that strontium nanolayer can combine with the micro structure of AH-Ti to form micro/nanosurface structure. Moreover, the sponge like network structure of AH-Ti can provide sufficient space to load enough strontium nanoparticles to form a biomimetic structure that helps long-term strontium ion release. According to previous studies, strontium had been doped to the titanium by alkali-heat treatment, of which the reaction solution included strontium chloride. Interestingly, the results showed better osteointegration in strontium-modified samples.[25] Moreover, strontium had been doped onto HA coating to enhance the osteogenic property, while the high degradation and unstable strontium ion release tended to compromise its application.[26] In addition, strontium had also been doped to titanium dioxide nanotubes (TNTs) by immersing it in 0.02 M $Sr(OH)_2$ solution, which showed enhanced osteogenic property in vitro and in vivo, while the TNTs coating was easy to be stripped.[27] Moreover, the above studies did not investigate the dose effects of strontium concentration and the relationship between the ion function and surface morphology was not assessed. Therefore, although both alkali-heat treatment and magnetron sputtering are conventional techniques for titanium surface modification, combination of these two methods to fabricate bionic surface was first found and the most suitable strontium titanate coating was able to be explored, which could provide reference information to support strontium relevant investigations. In this work, we kept the power of magnetron sputtering at 80 W, working pressure at 0.5 Pa, and temperature at 37°C for all the three groups, while the sputtering durations ranged from 30, 90, and 150 min. The following critical problems will be dissolved in our work: (1) the selection of the best sputtering duration which could endow the implant with the best osteogenic property; (2) confirming the strontium modified AH-Ti can promote osteointegration in vivo experiment; (3) discussing the role of ion function and surface topograph played in osteoblast function.

Materials and Methods

Materials

Titanium foils (purity: 99%; thickness: 0.5 mm; length: 10 mm; width: 10 mm) and titanium wires (diameter: 1 mm; length: 10 mm) were purchased from Advent Research Materials Ltd (Oxford, UK). NaOH solution was purchased from Aladdin Ltd (Shanghai, China). $SrTiO_3$ target material were purchased from Zhongnuo New Materials Ltd (Beijing, China). P-nitrophenyl phosphate assay kits were provided by Nanjing Jiancheng Bioengineering Institute Co., Ltd (Jiangsu, China).

Specimen Preparation

Titanium foils and wires were polished from (No. 400–800) SiC abrasive paper, ultrasonically washed with acetone, alcohol, and deionized water for 10 min subsequently. These pure Ti foils and wires were then dried by dry machine and kept in vacuum tube. As for AH-Ti, the pure Ti foils and wires were immersed in 5 M NaOH solution

and heated by oil bath at 80°C for 24 h and then washed with deionized water, dried and kept in a vacuum tube. The AH-Ti/Sr samples were prepared by magnetron sputtering device (Shenyang Kejing Auto-Instrument Co, Ltd, China) with the residual pressure no higher than $7*10^{-5}$ Pa, and the deposition working pressure was 0.5 Pa. The deposition process was performed at the power of 80 W with no additional heating in the chamber and kept the pulsing frequency as 60 kHz, while the deposition durations ranged from 30, 90, and 150 min and the samples were denoted as AH-Ti/Sr30, AH-Ti/Sr90, AH-Ti/Sr150 respectively. The pure Ti foils and AH-Ti were applied as the control group, and all the products were washed with ethanol and deionized water for two hours before use.

Surface Characterization

We used field-emission scanning electron microscopy (FE-SEM;HITA CHI, S-4800, Japan) to detect the surface morphology. The surface roughness was examined by atomic force microscopy (AFM; MultiMode 8, Karlsruhe, Germany). The ion concentration in the sample surfaces were determined by energy-dispersive X-ray spectroscopy (EDS; QX200, Brüker) and the distribution of strontium above the surfaces were monitored by EDS mapping. The hydrophilic property of samples was detected by water contact angle measurement which was conducted by the sessile-drop method at ambient temperature on a contact angle meter (SL200B, Solon). The crystal structure of different samples was detected by X-ray diffraction (XRD; D/Max-RB, Rigaku, Japan). The coating thickness was accessed by focused ion beam (FIB; Gatan, Ilion, USA) and field-emission scanning electron microscopy (FE-SEM; S-4800, Hitachi, Japan).

Ion Release Testing

Five samples of AH-Ti/Sr30, AH-Ti/Sr90 and AH-Ti/Sr150 were immersed in 5 mL PBS at 37°C with a thermostat. We took 1 mL solution and added 1 mL fresh PBS at the setting time point of 1, 4, 7, 14, 21, and 28 days, respectively. Next, the solution we collected was then diluted to 3 mL by PBS in order to detect the ion concentration which was measured by inductively coupled plasma atomic emission spectroscopy (ICP-AES; Optimal 8000, Perkin Elmer, USA).

In vitro Cytocompatibility Tests

Cell Culture

We used newborn mouse calvarial cells of line MC3T3-E1 in this work, which were purchased from ATCC (Manassas, VA, USA). The cells were supported by α-MEM (Gibco, Thermo Fisher) supplemented with 10% FBS (Gibco, Thermo Fisher), 1% penicillin/streptomycin (PS) (Beyotime, China) and incubated at 37°C in a 5% CO_2 environment. We purchased the RAW264.7 from Chinese Academy of Sciences (Shanghai, China), which were supported by DMEM (Gibco, Thermo Fisher) supplemented with 10% FBS (Bovogen, Australia), 1% penicillin/streptomycin (PS) (Beyotime, China).

Cell Morphology

The cell morphology experiment was conducted by staining at precise time points according to previous studies.[28] Cell morphology on different samples were confirmed by fluorescence microscopy (FM) and FE-SEMS-4800 (Hitachi). As for fluorescence microcopy observation, cells on samples were fixed by 4% paraformaldehyde (Sigma, USA) for an hour after three days of cell culture and then stained by phalloidin (Beyotime, China) for an hour and DAPI (Beyotime, China) for 15 min respectively. Accordingly, the cell morphology was detected by FM (Olympus IX71, Japan) after washing three times for background staining elimination. The cell areas and cell aspects ratio were analyzed by Image J (1.51).

The SEM observation of cells on different samples was also performed. Briefly, after three days of cell culture, the cells on specimens were fixed by 2.5% glutaraldehyde (Solarbio, China) for six hours, washed with PBS and gradient dehydration by 30%, 50%, 70%, 90%, and 100% alcohol respectively. Next, the 100% alcohol was replaced by Butyl alcohol (Sigma, USA) for 10 min, dried at room temperature and observed by field-emission scanning electron microscopy (FE-SEMS-4800 (Hitachi) after gold sputtering.

Cell Viability

The MTT method was carried out to detect the cell viability. After four and seven days of cell culture, the incubated medium was replaced by 300 μL 10% MTT solution (Solarbio, China) diluted by α-MEM. Then, 300 μL DMSO was used to replace the MTT solution after four hours of cell culture. One hundred microliters of solution from each well was absorbed into 96-well plates (Corning Incorporated, USA). The results were detected by microplate reader (Bio-Rad 680, USA) at a wavelength of 490 nm.

Alkaline Phosphatase (ALP) Activity Assay

The ALP activity was detected by alkaline phosphatase assay kit (Nanjing Jiancheng Bioengineering Institute, China) and BCA protein assay kit (Beyotime, China).

Briefly, the cells cultured on different samples were collected after osteogenic induction for seven and 14 days. We used cell lysis buffer (Beyotime, China) to lysis cells and put into 4°C refrigerator for 50 min. Thirty microliters of cell lysis solution on each well was used in detection by ALP kit and the absorbance was read at the wavelength of 520 nm by microplate reader (Bio-Rad 680, USA). Meanwhile, 20 μL of cell lysis solution on each well was used in detection by BCA protein assay kit and the absorbance was read at a wavelength of 562 nm by microplates reader (Bio-Rad 680, USA). The final ALP activity was normalized by protein concentration and expressed in nanomoles of p-nitrophenol produced per milligram of protein per minute.

Matrix Mineralization

We used alizarin red staining to determine the contents of matrix mineralization. Briefly, we collected the samples after 14 days of osteogenic induction by osteogenic medium (α-MEM, 100 nM dexamethasone, 10 mM beta-glycerol phosphate, and 50 μg/mL ascorbic acid). The cells on the samples were fixed by 4% paraformaldehyde for 40 min. Afterwards the fixed cells were washed thrice with PBS and stained by 40-mM alizarin red (pH=4.2) staining at room temperature for 60 min. Next, the extra staining was washed with deionized water. Accordingly, the mineralized calcium nodules were dissolved by 10% cetylpyridinium chloride (Sigma, USA) and 200 μL solution from each well were absorbed into 96-well plates and detected by microplates reader (Bio-Rad 680, USA) at the wavelength of 540 nm.

Osteocalcin (OCN) Concentration

The cells were collected after 14 days of osteogenic induction and the cell lysis was performed by lysis buffer. Next, the liquid were centrifugated with the speed of 12,000 rpm for 10 min. The supernatant was used to do the detection by OCN ELISA kit (Jining Shiye, China). The optical density was analyzed by microplates reader (Bio-Rad 680, USA) with the wavelength of 450 nm.

qRT-PCR Assay

We analyzed the osteogenic related gene expression by qRT-PCR after culturing pre-osteoblast cells (MC3T3-E1) for 14 days of osteogenic induction. Herein, we selected the five osteogenic relevant premiers such as type-1 collagen (Col-1), ALP, osteopontin (OPN), osteocalcin (OCN), *RUNX2* and osteoclast related genes as *RANKL* and *TRAP* for quantitative reverse transcription quantitative real time polymerase chain reaction (qRT-PCR). In short, $3*10^4$ cells were inoculated per well and cultured for two weeks. In addition, rh*RANKL* (50 ng/mL) was added in RAW264.7 culture medium to induce osteoclastogenesis.The cell biomass from five selected samples within each group (Ti, AH-Ti, AH-Ti/Sr30, AH-Ti/Sr90, AH-Ti/Sr150) were collected. Cells were lysed by using Trizol (Invitrogen) and the total mRNA was collected by RNA extraction kit (Thermo Fisher), of which the concentration was detected by Nanodrop (Thermo Fisher). 20μLof RNA from each group was reverse transcribed to synthesized cDNA by using the PrimeScript™ RT Master Mix (Perfect Real Time, Takara, China). The TB Green® Premix Ex Taq™ kit (Takara Biotechnology, Japan) combined with qRT-PCR analysis device (Applied Biosystem 7500) were performed to detection. The sequences of different primers we used in this step were displayed in Table 1 and the *GAPDH* was used as the reference gene.

In vivo Experiment

A total of 80 female adult Sprague Dawley rats (weight 220–250 g) provided by animal center of Wenzhou Medical University were used in this experiment which was approved by the Wenzhou Medical University Animal Care and Use Committee, and all procedures strictly

Table 1 Real-time Polymerase Chain Reaction Primers used in this Study

Target Genes	Primers
ALP	F:5'-AGCGACACGGACAAGAAGC-3' R:5'-GGCAAAGACCGCCACATC-3'
COL-I	F:5'-CCTGAGCCAGCAGATTGA-3' R:5'-TCCGCTCTTCCAGTCAG-3'
OPN	F:5'-GACAGCAACGGGAAGACC-3' R:5'-CAGGCTGGCTTTGGAACT-3'
RUNX2	F:5'-AACAGCAGCAGCAGCAGCAG-3' R:5'-GCACGGAGCACAGGAAGTTGG-3'
OCN	F:5'-AGATTGTTGGGGCACAAGGT-3' R:5'-CCTTCAGCAGGGAAACCGAT-3'
RANKL	F:5'-CTGAGGCCCAGCCATTTG-3' R:5'-GGAACCCGATGGGATGCT-3'
TRAP	F:5'-CCAATGCCAAAGAGATCGCC-3' R:5'-TCTGTGCAGAGACGTTGCCAAG -3'
GAPDH	F:5'-GGCATTGCTCTCAATGACAA-3' R:5'-TGTGAGGGAGATGCTCAGTG-3'

followed the committee's ethical guidelines. The castration surgery was performed to 40 female rats when the weight of rats reached 200 g, and the other 40 female rats without surgery used as normal model. Next, all rats were fed in specific pathogen free (SPF) conditions. We followed the protocols approved by the ethics committee for animal experiments of Wenzhou Medical University to carry on the surgical procedures. AH-Ti (40 implants; 20 for normal rats model and the other 20 for osteoporotic rats model), AH-Ti/Sr90 (40 implants; 20 for normal rats model and the other 20 for osteoporotic rats model) AH-Ti (40 implants), AH-Ti/Sr90 (40 implants) were applied to investigate the osteointegration in vivo. The bone defect experiment was conducted by preparing pile road (diameter: 1 mm, length: 10 mm) in the femur of the normal and osteoporotic rats. Next, two types of implants were inserted into the pile road of the femur (one implant per femur) sequentially. Finally, the opening skin was sutured and sterilized by 75% alcohol. After four weeks of bone healing, the rats were killed by overdose of anesthetic and the femurs were acquired for further examination.

Micro-CT Evaluation

The acquired femurs were maintained in 4% paraformaldehyde solution for two days and then washed with PBS three times. After washing, six samples of these femurs were dried and wrapped using sealing film for further analysis, which was applied to protect the bone tissue. All the femurs from each group were scanned by three-dimensional (3D) scanning in a computed tomography (CT) system (μCT80, Switzerland); an integration time of 300 ms was selected at 80 kV and 114 mA, the reconstruction of the A constrained 3D Gaussian filter for noise suppression was used to reconstruct the 3D images (10 mm isotropic voxel) for qualitative and quantitative evaluation. The new bone formation around different implants were investigated and about 1 mm below the epiphyseal line used as specific analysis area. We estimated the mean trabecular number (Tb.N), the bone volume per total volume (BV/TV), the mean trabecular separation (Tb.Sp), the mean trabecular thickness (Tb.Th), and the mean connective density (Conn.Dens).

Histological Analysis

The samples were fixed in 4% paraformaldehyde after pushing out the implant. Afterwards, the gradual ethanol (70%, 90%, 95%, and 100%) dehydration was performed. We infiltrated the dehydrated samples with xylene and embedded in poly (methyl methacrylate) before preparing undecalcified sections. Next, we prepared the undecalcified sections (around 70 μm). Then, these sections were stained with H&E staining and Masson staining. Fluorescence microscopy observation was conducted to analyze the new bone formation.

Statistical Analysis

The samples used in each experiment are independent, and the same samples are not used in different tests. All data in the experimental results were repeated independently more than three times and expressed as mean ±SD, and statistical analysis was performed using GraphPad Prism 7 software, ANOVA, and paired *t* test, with a confidence level of 95% ($p<0.05$) and 99% ($p<0.01$).

Results and Discussion

Surface Characterization

The SEM results of samples with different coating parameters were depicted in Figure 1. The obvious scratch already presented on the sample surface, was formed by mechanical polishing.[29,30] The alkali-heat treated titanium (AH-Ti) exhibited a sponge network structure, which was in agreement with previous findings.[31] It could be observed that the nanowires of the sponge structure were thicker after the deposition of $SrTiO_3$ and numerous nanoparticles could be found on AH-Ti/Sr specimens. Moreover, the nanolayers became thicker with the increase of sputtering durations (AH-Ti/Sr150 >AH-Ti/Sr90 >AH-Ti/Sr30). The AFM results in Figure 1 reflected the Ra value of AH-Ti (44.6.3 ±4.2 nm) was significantly higher than Ti (20.3±3 nm), while there is no significant difference after strontium modification. It could be attributed to the fact that the formation of sodium titanate layer was significantly increased after hot-alkaline treatment, even though sputtering did not statistically alter the surface roughness.[31] According to previous studies, the surface roughness and wettability alternation would cause the response of osteoblast cells and influence the osteointegration.[32–34] EDS mapping analysis showed the element composition of the sample surface. As shown in Figure 3A, only Ti and O element could be detected on the pure Ti surface, and the 17.23at% of O element was attributed to the oxidation of Ti surface. In addition, the Na element could be detected on the hot-alkaline treated specimens, which was attributed to the sodium titanate layer doped with Na ion from NaOH solution.[31] The detection of Sr element on strontium modified specimens confirmed the success coating of strontium layer, and the Sr signal became

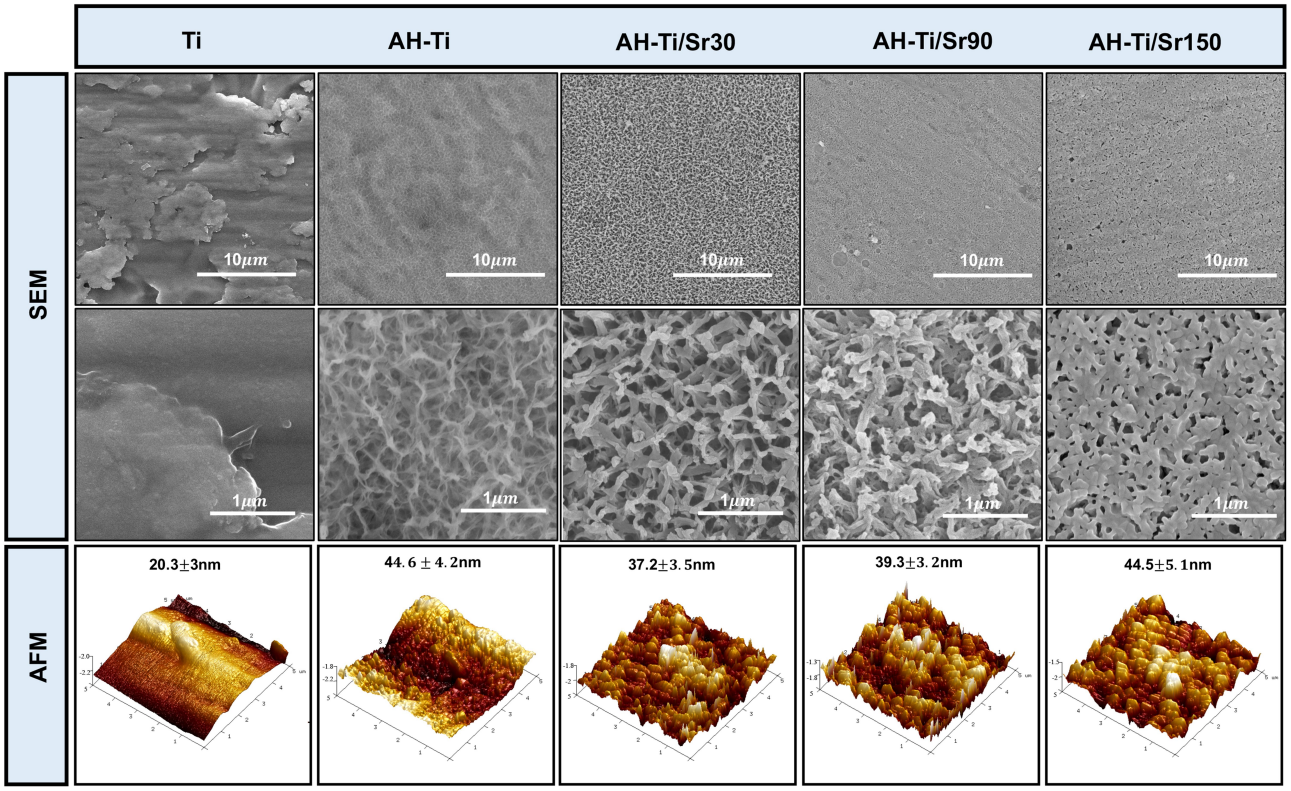

Figure 1 Top view SEM images and AFM 3D images of different samples.

stronger with the increase of the duration (2.01at% >1.2at% >0.92at%). The XRD patterns of the strontium modified samples were shown on Figure 2. Even after the hydrothermal reaction and magnetron sputtering, the peaks from the $SrTiO_3$ and amorphous sodium titanate can not be observed. The fact that the crystal structure would not be altered might be attributed to the coating layer, which was too thin to be detected.[35] In addition, the water contact angle measurement was performed to show the hydrophilic/hydrophobic ability of different specimens, which was shown in Figure 3B. The contact angle on the Ti approximately is 63.5±3.5°, while the AH-Ti became super hydrophilicity after the hot alkaline treatment and the contact angle is 12.1±1.5°. This phenomenon was attributed to the increased surface roughness. Studies had proved that the surface roughness is relevant to water contact angle measurement, and the increased surface roughness will enhance the surface hydrophilic.[35] However, the contact angle was increased obviously after the sputtering of $SrTiO_3$ (AH-Ti/Sr), which reached almost 100° and there is no significant difference between the $SrTiO_3$ modified three groups. This phenomenon was attributed to the narrowed aperture and the accumulation of $SrTiO_3$ nanocoating on the sponge-like surface, which was confirmed by previous studies that the smaller the aperture, the more hydrophobic it would be.[36,37] Focused ion beam and field-emission scanning electron microscopy were conducted to show the cross sectional images of specimens (Figure 4). The cross section of AH-Ti showed numerous needles like structure with many gaps which was blunt in AH-Ti/Sr30 because of the covering of thin $SrTiO_3$ coating. Moreover, the coating thickness of $SrTiO_3$ in AH-Ti/Sr30 is 100±6 nm, which is thin and

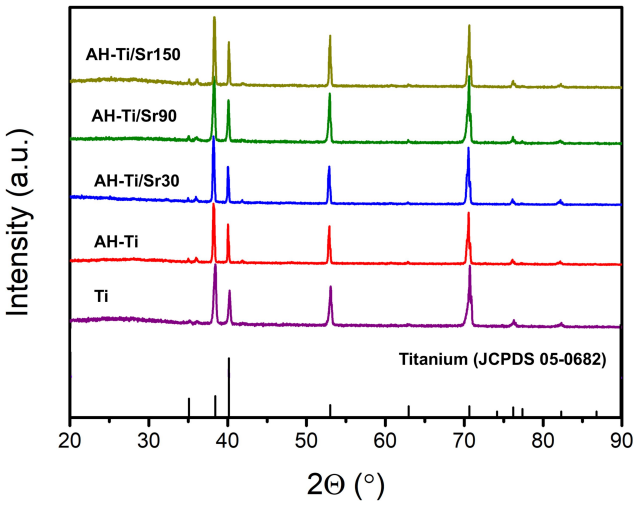

Figure 2 XRD patterns of different samples.

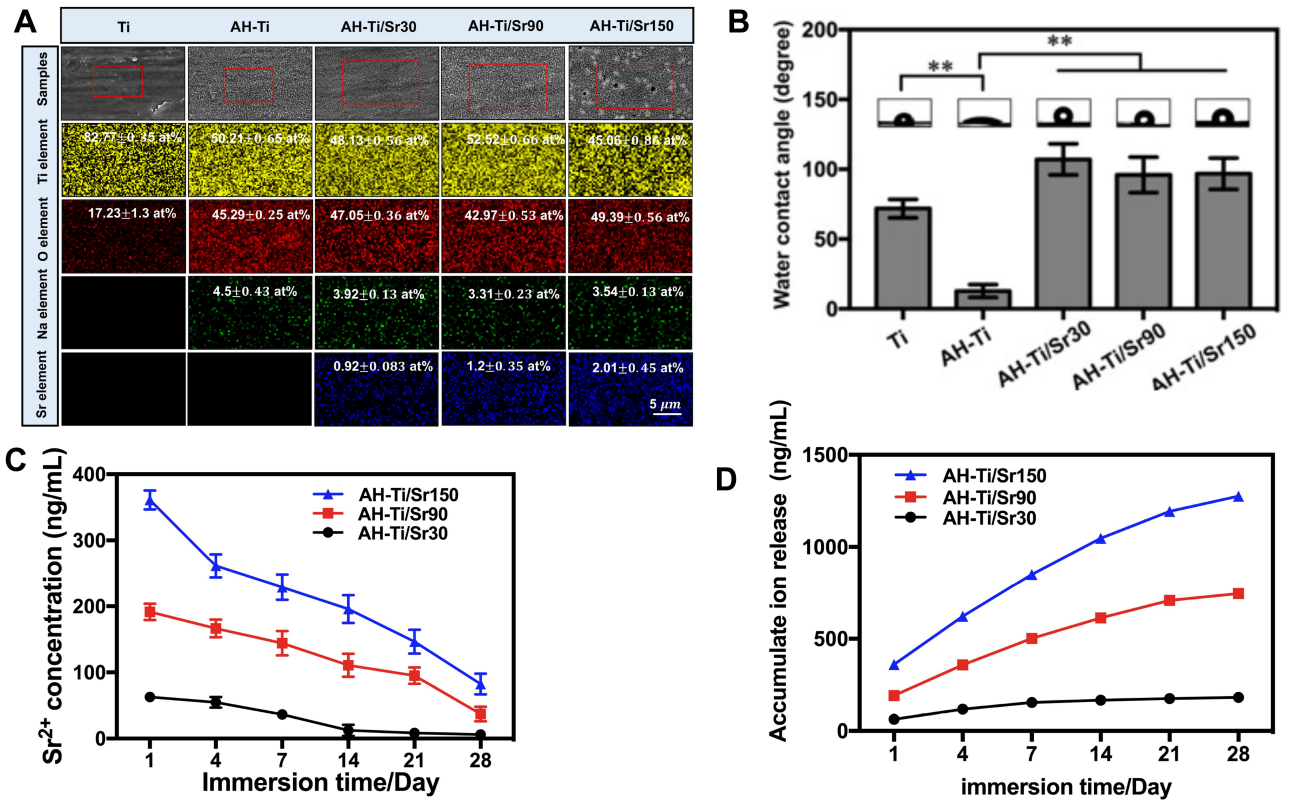

Figure 3 (**A**) EDS mapping of the area enclosed by a square in SEM images showing the distribution of Ti, O, Na, and Sr elements (n=6). (**B**) Water contact angle measurement of different specimens (n=6), *P<0.01. (**C**) The released profiles of Sr^{2+} from AH-Ti/Sr substrates within 28 days (n=6). (**D**) The accumulated Sr^{2+} concentration from AH-Ti/Sr substrates within 28 days (n=6).

difficult to detect on irregular surfaces. In addition, the cross section of AH-Ti/Sr90 showed clear $SrTiO_3$ coating of 300 ±16 nm, which was intermittent and looked like sticks maybe due to the sponge like surface structure of AH-Ti.

Strontium ion release from AH-Ti/Sr during the 28 days was shown in Figure 3C and D. We observed that the released Sr^{2+} from AH-Ti/Sr150 was higher than that of AH-Ti/Sr90 at any period of immersion time. Similarly, the released Sr^{2+} from AH-Ti/Sr90 was higher than that from AH-Ti/Sr30. In addition, the accumulation concentration on three groups over the full 28 days were 1275.75 ng/mL, 745.45 ng/mL, and 181.32 ng/mL,

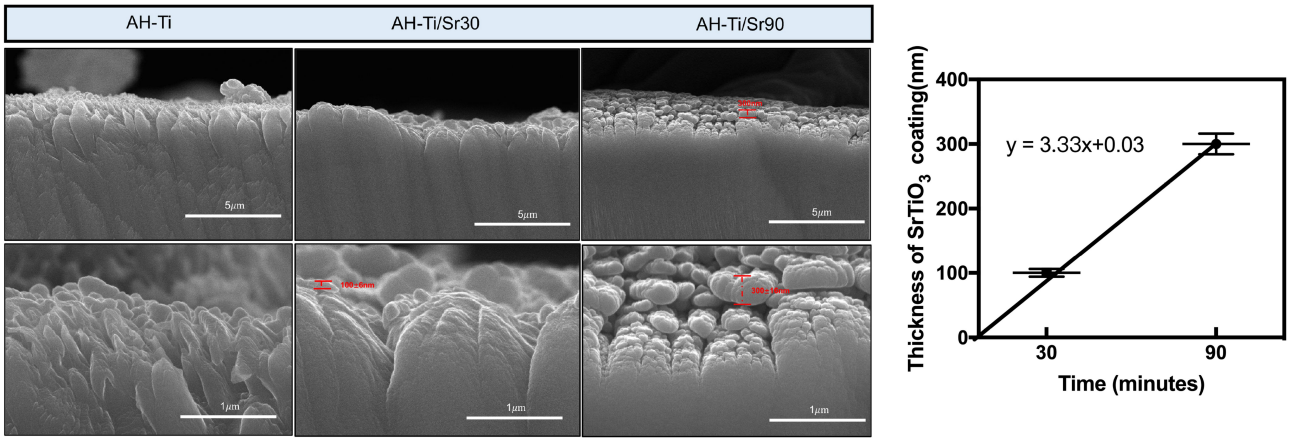

Figure 4 Cross-sectional SEM images and thickness statistics of $SrTiO_3$ coatings of 30 and 90 min.

respectively (Figure 3D). We could conclude from the ion release test that the ion was released faster and for a more prolonged time by the increase of sputtering durations (AH-Ti/Sr150 >AH-Ti/Sr90 >AH-Ti/Sr30) and the reason was mainly attributed to the Sr element amount above the sample surfaces (AH-Ti/Sr150: 2.01at% >AH-Ti/Sr90:1.2at% >AH-Ti/Sr30: 0.92at% from EDS mapping analysis).

In vitro Cell Experiment

Cell Compatibility

We used FM staining and SEM to observe the cell morphology on the sample surface (Figure 5A). From the spread area we observed that the cells were spread thinner and showed shrink body on AH-Ti and AH-Ti/Sr150 specimens, while the cells on Ti, AH-Ti/Sr30 and AH-Ti/Sr90 showed broad cell area and no significant difference was observed between

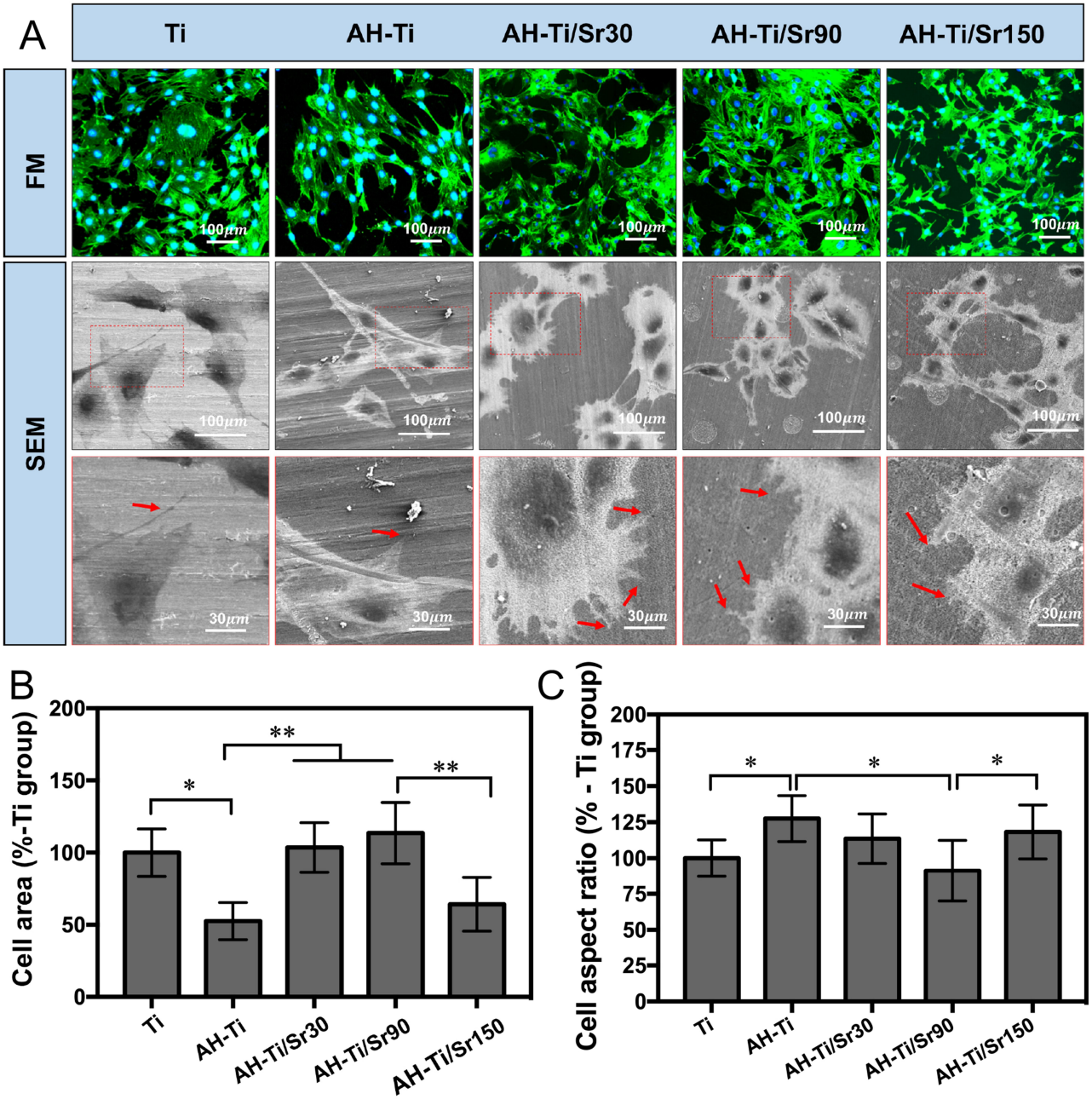

Figure 5 (**A**) Cell morphology of MC3T3-E1 on different samples observed by FM and SEM (n=6). (**B**) The statistical analysis of cell area, **P*<0.05, ***P*<0.01. (**C**) The statistical analysis of cell aspect ratio, **P*<0.05, ***P*<0.01.

these three groups, which was statistically analyzed and displayed in Figure 5B. In addition, the cells on AH-Ti and AH-Ti/150 showed increased cell aspect ratio compared with Ti and AH-Ti/90 (Figure 5C). The cell behavior on AH-Ti may be ascribed to two reasons including the release of Na ions which can compromise the cell condition,[38] and the microstructure which has been proved to decrease the cell spread area.[37] The same inferior cell behavior on AH-Ti/Sr150 was attributed to the excess amount of Sr, while the Sr amount on AH-Ti/Sr30 and AH-Ti/Sr90 was within the noncytotoxic level.[39] In addition, the AH-Ti/Sr groups (AH-Ti/Sr30, AH-Ti/Sr90, AH-Ti/Sr150) exhibited more stress fibers and actin microfilaments than control groups (AH-Ti, Ti), indicating the function of nanolayer formed by magnetron sputtering endowed the surface with numerous nanoscale cell attachment sites. Notably, the AH-Ti/Sr90 group showed the most number of plate synapse and filamentous pseudopodia (Figure 5A red arrow) which had been proven to be conducive to cell growth and osteogenic differentiation.[40] Therefore, we could conclude that the micro/nanostructure could be conducive to the intimate intercellular interaction. Consequently, the biomimetic surface substrates (AH-Ti/Sr90) provided the most advantageous environment for osteoblast growth, which was critical to osteogenic differentiation. The cell morphology of RAW264.7 was observed in Figure 7A. In contrast to the MC3T3-E1 observation, the RAW264.7 seemed assembled and flat in AH-Ti/Sr groups, while it was dispersed and stereoscopic in control groups Ti and AH-Ti.

The cell viability of the materials was assessed by MTT which was shown in Figure 6A. It showed that the optical density of the hot alkaline treated group (AH-Ti)

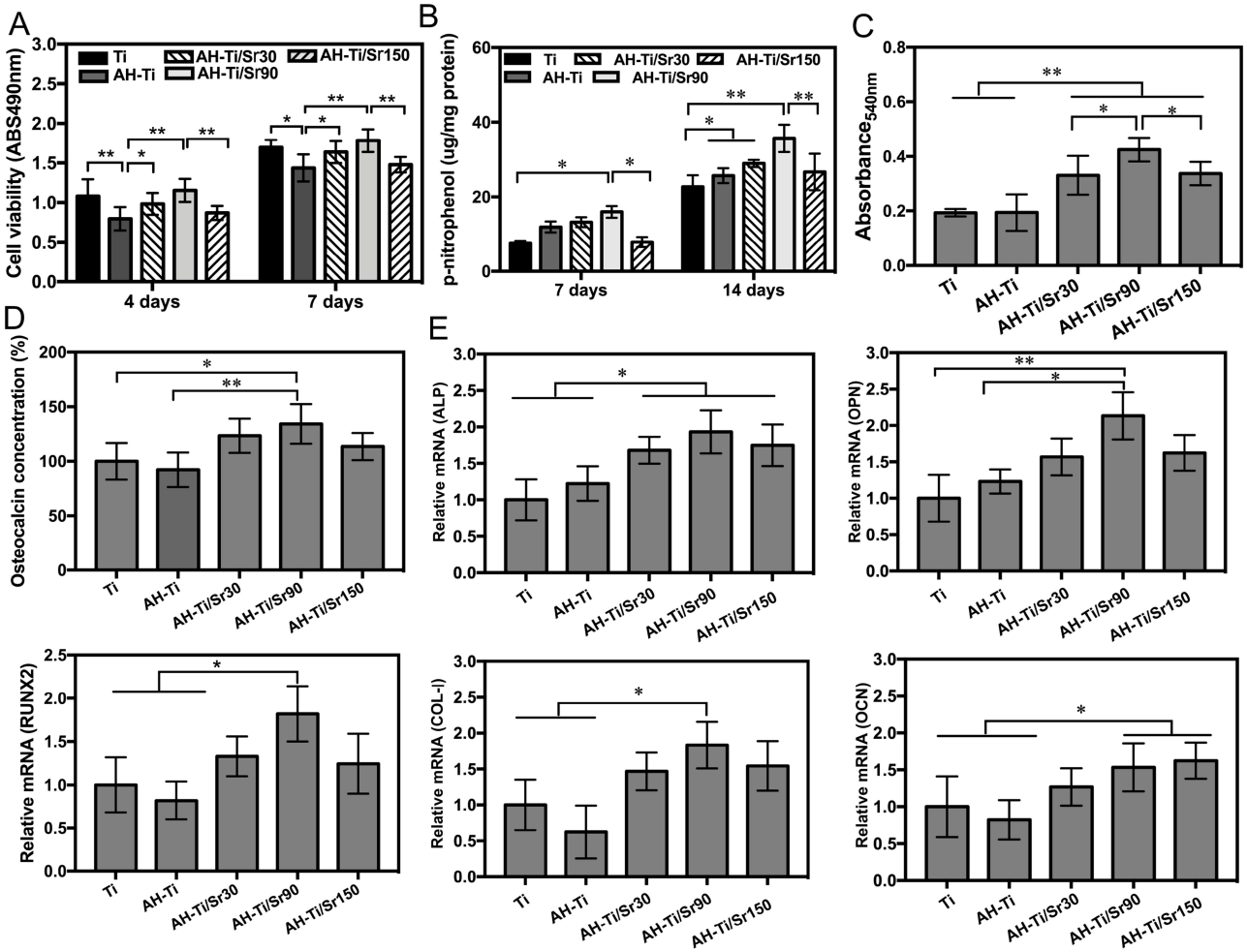

Figure 6 (**A**) Cell proliferation of MC3T3-E1 on different samples after four and seven days of cell culture (n=6). (**B**) ALP activity of MC3T3-E1 on different samples after seven and 14 days of osteogenic induction (n=6). (**C**) Mineralization level of MC3T3-E1 on different samples after 14 days of osteogenic induction (n=6). (**D**) OCN concentration of MC3T3-E1 on different samples after 14 days of osteogenic induction (n=6). (**E**) The osteogenic related gene expression of different samples at seven days (n=6). *P<0.05, **P<0.01.

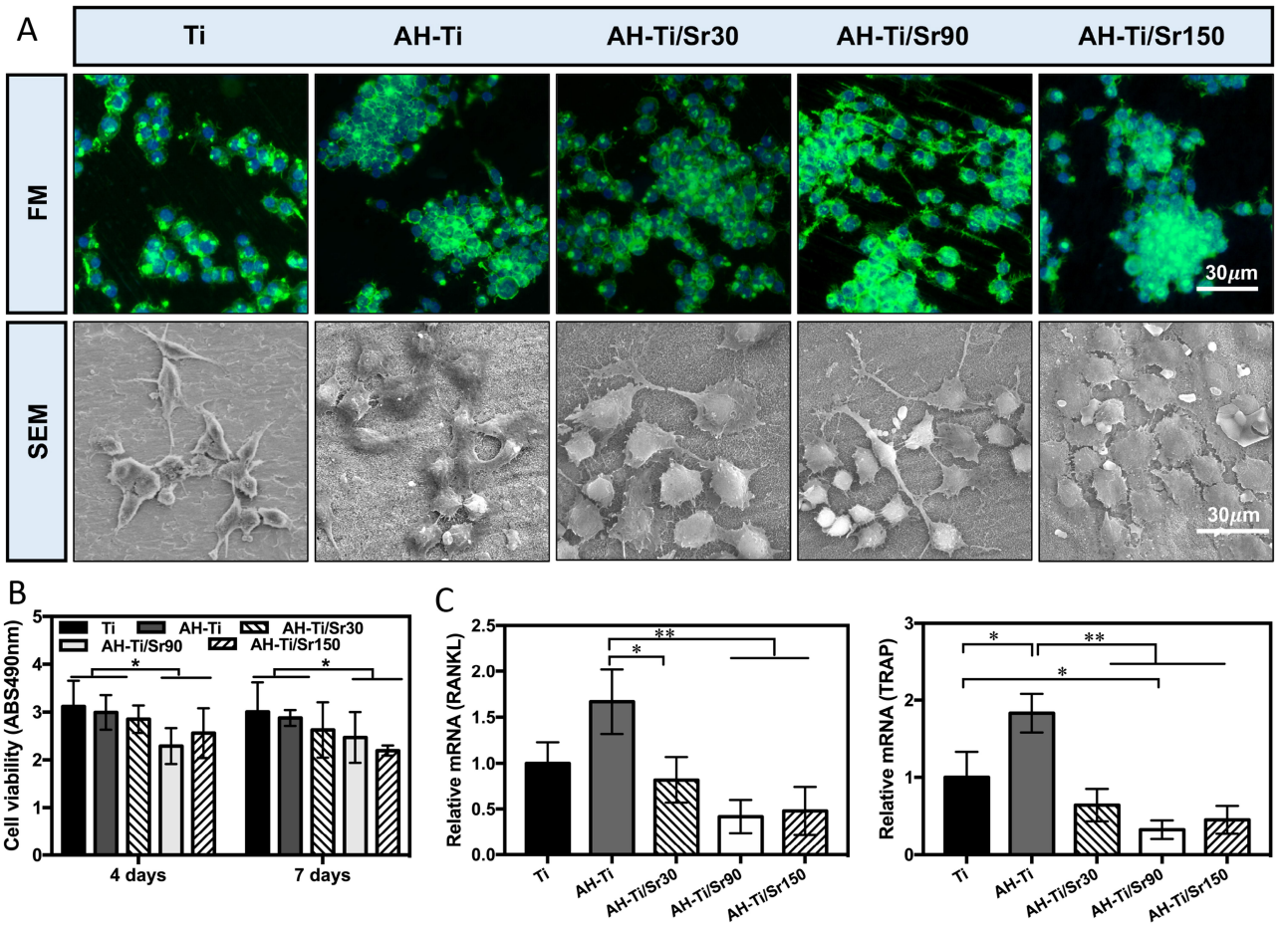

Figure 7 (**A**) Cell morphology of Raw264.7 on different samples observed by FM and SEM (n=6). (**B**) Cell viability of Raw264.7 on different samples after four and seven days of cell culture (n=6). (**C**) The relative expression of *RANKL* and *TRAP* genes of Raw264.7 on different samples (n=6). **P*<0.05, ***P*<0.01.

was lower than Ti, indicating the inferior cell viability on AH-Ti substrates. The result corresponded to cell observation and the cell viability was influenced by cell growth behavior. The OD increased after the deposition of $SrTiO_3$, indicating a better cell viability which was attributed to the release of strontium and the alternation of surface structure.[37] Whatis more, the AH-Ti/Sr90 group showed the highest optical density, while it was decreased in the AH-Ti/Sr150 group. Both the cell proliferation in four and seven days showed the same trend. On the one hand, the trabecular bionic surface in AH-Ti/Sr90 group regulated the cell behavior and provided advantageous circumstance for cell growth. On the other hand, the relatively decreased Na element on strontium modified substrates according to EDS mapping (Figure 3A) might be another reason that was conducive to cell viability. As for titanium ions, it can both promote the osteoclastogenesis and inhibit the cell proliferation and differentiation of osteoblast and thus impair the osteointegration.[41,42] Besides, it had been proved that the Ti^{4+} would decrease the activity of VECs, which through the active Akt/IKKα/β pathway and p38 dephosphorylation to promote the expression of endogenous reactive oxygen species and oxidative damage membranes in VECs and finally induce cell apoptosis.[43] However, though it is inert and easy to form oxide film to protect titanium, researchers had proved that the titanium oxide film could be degraded and release titanium ion.[44] Moreover, the dissolution and repair of the oxide film are in dynamic equilibrium, which regulate the biocompatibility of titanium implant surface. In conclusion, the titanium ion released too few to influence the cell viability due to the slow degradation of titanium oxide film and the almost same level of titanium element (Figure 3A) showed by the EDS mapping. Therefore, Sr^{2+} played pivotal role in cell behavior regulation. From ion release test, the amount of Sr^{2+} released from AH-Ti/Sr150 (622ng/mL) was approximately 1.73-fold that from AH-Ti/Sr90 (358.2 ng/mL) over the first 4four days of immersion (Figure 3D).

Because of the triple dilution in the method of ion detection, the Sr^{2+} concentration in cell condition of 24well plates would be 1866ng/mL in AH-Ti/Sr150 and 1074.6ng/mL in AH-Ti/Sr90 over the first four days. According to previous studies, the optimum Sr^{2+} had been confirmed to benefit cell proliferation, while the concentration more than 1400 ng/mL would have an adverse effect on osteoblast proliferation.[39,45,46] Ion release in AH-Ti/Sr150 (1866 ng/mL) exceeds the threshold from other studies (1400ng/mL) while it was still within the advantageous concentration from AH-Ti/Sr90 (1074.6ng/mL). Thus, our results were consistent with previous study. The cell viability results of RAW264.7 was shown in Figure 7B. In contrast to the MC3T3-E1, the cell viability was decreased on the strontium modified samples. Compared to the AH-Ti and pure Ti, the AH-Ti/Sr90 and AH-Ti/Sr150 group showed statistically low cell viability ($P<0.05$), which indicated the activity of osteoclast precursor was inhibited on these two groups. The results indicated that the strontium ion release could hinder the osteoclastogenesis which was consistent with previous studies.[23,47–49]

Cell Differentiation

The ALP activity is the early marker of cell differentiation,[30] which was assessed quantitatively. Results in Figure 6B showed that the AH-Ti slightly promoted the ALP activity both at seven and 14 days, which was consistent with previous studies.[50] Though previous studies had proved that the microstructure of AH-Ti could promote the ALP activity, our results confirmed that the function of surface topography alone to enhance osteogenesis was limited and was consistent with some studies.[30,50] In addition, the ALP activity increased markedly after the deposition of suitable $SrTiO_3$ (ALP activity in AH-Ti/Sr150 was decreased), especially in the AH-Ti/Sr90 group which showed the highest ALP activity both at seven and 14 days. This phenomenon was attributed to two reasons. On the one hand, the AH-Ti/Sr90 surface from SEM (Figure 1) showed the bone imitated structure, which had been confirmed to be able to stimulate the cell differentiation.[51] On the other hand, the accumulated strontium release (Figure 3D) of AH-Ti/Sr90 at seven and 14 days was significantly lower than that of AH-Ti/Sr150, of which the concentration is conducive to osteogenic differentiation. Therefore, the appropriate strontium ion concentration provided an advantageous circumstance for cell differentiation, of which the mechanism is by a calcium sensing receptor (CaR) dependent mechanism.[22]

The extracellular matrix mineralization and OCN concentration were the main markers of the osteoblast differentiation and were measured to reflect the late stage of osteogenic differentiation.[45] The results in Figure 6C showed that the deposition of strontium promoted the mineralization level, and the AH-Ti/Sr90 group exhibited the statistically highest mineralization level compared with other groups (Ti, AH-Ti, $P<0.01$; AH-Ti/Sr30, AH-Ti/Sr150, $P<0.05$), which was consistent with ALP activity. Interestingly, compared to AH-Ti and pure Ti both the AH-Ti/Sr30 and AH-Ti/Sr150 groups promoted the extracellular mineralization ($P<0.01$), though there was no significant difference between two groups. The OCN concentration experiment (Figure 6D) also showed that the OCN concentration of the AH-Ti/Sr90 group statistically higher than that of control groups (Ti and AH-Ti; Ti, $P<0.05$; AH-Ti, $P<0.01$). In addition, the OCN concentration of the AH-Ti/Sr30 group and the AH-Ti/Sr150 group was slightly higher than that of the control groups though there is no significant difference. However, the AH-Ti showed no promotion to mineralization and OCN concentration compared to pure Ti group. These results indicated that strontium ion release played a pivotal role in extracellular mineralization and OCN concentration.The qRT-PCR was used to further determine the osteogenic differentiation and anti-osteoclast activity at the genetic level. The results in Figure 6E, showed the osteogenic related gene expression. After 14 days of cell culture, it seemed that only the ALP and OPN were upregulated after the treatment of hot-alkaline (AH-Ti), though there was no significant difference ($P>0.05$) among them. This result corresponded to the ALP activity and mineralization, indicating that microstructure is inadequate to promote the osteogenic differentiation. Accordingly, compared to the AH-Ti, the osteogenic related gene expression including *ALP*, *RUNX2*, *OCN*, *OPN* and *COL-1* was statistically upregulated on AH-Ti/Sr90 substrates ($P<0.05$), which showed the most superior osteogenic differentiation ability. It exhibited that the AH-Ti/Sr90 substrates had the most suitable ion release property and surface topography, of which the robust synergistic function had been confirmed by Yao et al.[52] In addition, the ALP expression was also statistically upregulated on AH-Ti/Sr30 and AH-Ti/Sr150 compared to AH-Ti and pure Ti (<0.05), which was mainly ascribed to the surface topography. According to previous studies, the cell proliferation and adhesion had

important effects on osteogenic differentiation and regulate the osteogenic related gene expression.[53] The micro/nano bone imitated surface which formed by microstructure (hot alkaline treatment) and nanostructure (magnetron sputtering), promoting the cell spread and cell proliferation.[54,55] As concluded in the cell morphology and cell viability experiment (Figures 6A and 7A), the AH-Ti/Sr90 group promoted cell spread and cell viability to the greatest extent. From the above assessments, the surface of AH-Ti/Sr90 was bionic and the suitable strontium ion release provided the most advantageous circumstance for cell differentiation. Thus, we speculated that the micro/nanostructure, strontium ion, combined with the cytocompatibility had a synergistic effect on osteogenic related gene regulation. Consequently, the AH-Ti/Sr90 group showed the highest ALP activity at an early stage, the highest mineralization level and OCN concentration at late stage. Accordingly, the osteoclast specific genes (*RANKL*, *TRAP*) expression was evaluated by RAW264.7 cells cultured on different substrates with the cell seeding density of $5*10^4$/mL. In consistence with the cell viability of osteoclast which was inhibited in strontium modified specimens (Figure 7B), the osteoclast differentiation relative gene expression was downregulated. As shown in Figure 7C, compared to Ti group and AH-Ti group, the *RANKL* expression was downregulated in strontium modified samples (AH-Ti/Sr). Interestingly, compared to AH-Ti, the AH-Ti/Sr30 group was downregulated by 1.8-fold, the AH-Ti/Sr90 and the AH-Ti/Sr150 group were downregulated by 3.2-fold. *TRAP* expression in AH-Ti was upregulated by 1.82-fold compared to the Ti group. However, the *TRAP* expression in AH-Ti/Sr30 was downregulated by 2.2-fold, while AH-Ti/Sr90 and AH-Ti/Sr150 were downregulated by 4.65-fold and 3.1-fold respectively. These results indicated that the AH-Ti/Sr could inhibit the osteoclast related markers (*RANKL*, *TRAP*) in RAW264.7 due to the strontium ion release which could produce negative effects on osteoclast viability by (CaR) dependent mechanism, and thus decrease the resorbing activity.[23]

In conclusion, the AH-Ti/Sr90 group which possessed bone-bio-mimic surface structure and suitable ion release property had a synergistic effect on osteogenic induction and osteoclast inhibition and thus made implants osteoconductive and osteoinductive. Though some studies had studied the function of strontium, the best thickness of $SrTiO_3$ coating was proved for the first time by the above in vitro experiment.

In vivo Experiment

Micro-CT

We had confirmed that AH-Ti/Sr90 was the best group as indicated by results from in vitro cell experiments, and numerous studies had compared the AH-Ti and pure Ti in animal experiment.[51] Thus, we further used AH-Ti and AH-Ti/Sr90 groups for in vivo experiment to determine the bone-to-implant osteointegration. The in vivo experiments usually waited four and 12 weeks of bone healing to detect the bone formation in many papers.[56,57] According to studies, the callus reconstruction was completed after four weeks and the lamellar bone was reconstructed via the activity of a Haversian system, which means the new bone was completely formed after four weeks.[58] Therefore, we thought that the detection of new bone formation after four weeks of bone healing was enough to reflect the bone-to-implant osteointegration. Compared to the normal groups, the osteoporotic bone density and bone volume decreased obviously as shown in Figures 8 and 9, which confirmed the successful fabrication of the osteoporotic model. From the osteoporotic rat model, we found that the AH-Ti/Sr90 group had significantly more new bone formation and higher bone density around the implant fixation than the AH-Ti group both in callus and medullary cavity, of which the BV:TV ratio was 1.8-fold higher, the Tb.N was 1.92-fold higher, and Conn-Dens was 2.55-fold higher, while there was no significance between groups about Tb.Th. In addition, the Tb.Sp in AH-Ti/Sr90 group was 1.5-fold lower compared to the AH-Ti group. However, in the normal model, only the BV:TV ratio and Conn-Dens in AH-Ti/Sr90 group was statistically higher than AH-Ti, which was 1.54-fold and 1.3-fold higher compared to AH-Ti, respectively. The results indicated that the AH-Ti/Sr90 group could enhance the bone volume and osteointegration in normal conditions and the promotion was more effective in osteoporotic conditions. Appropriate strontium concentration regulated the cell behavior, of which the mechanism had been proved by previous studies. Sr^{2+} has the similar structure with Ca^{2+}, which means the same target with Ca^{2+}, and thus the CaR pathway plays an important part in biofunction regulation.[59] On the one hand, strontium could activate intracellular calcineurin and increase the nuclear transport of NFATc1, which enhanced the expression of wnt5a, activated Ryk/RhoA and thus increased the cell proliferation and duplication of osteoblast.[60] On the other hand, strontium activate the CaSR/PI3K/Akt signal pathway, prevent the synthesis of GSK3 by glycogen and the expression of β-catenin

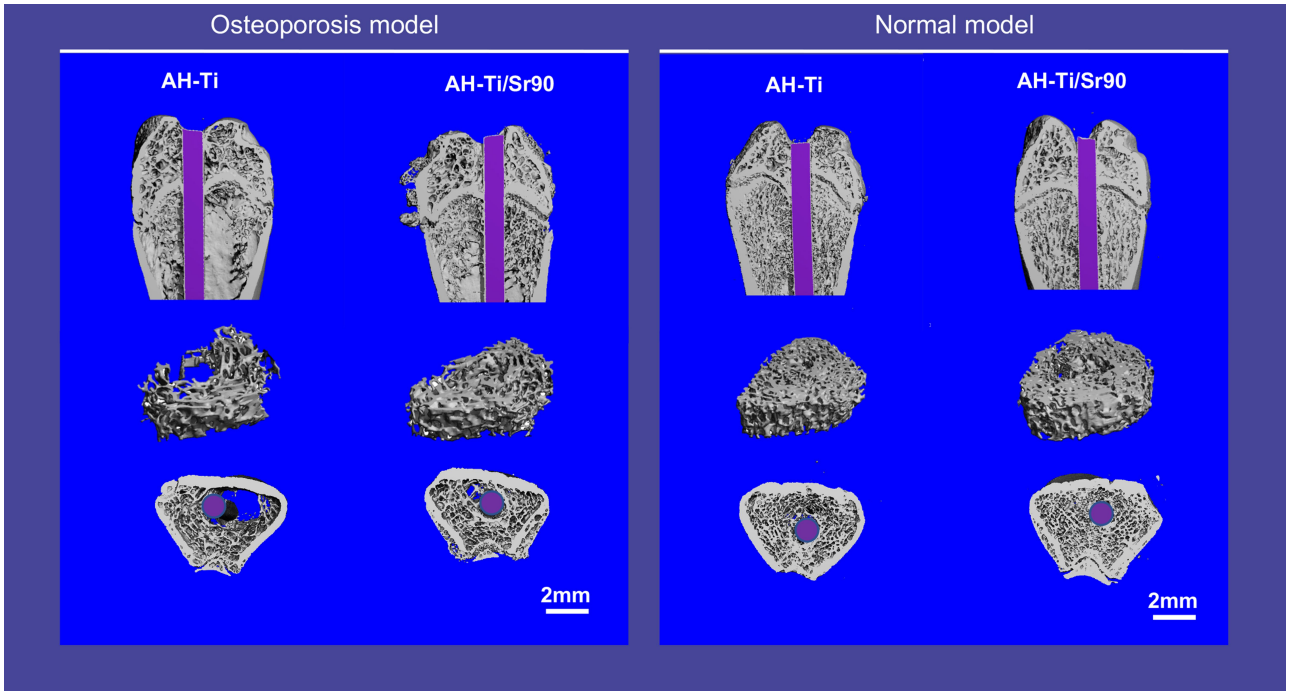

Figure 8 Micro-CT images of reconstructed 3D models of surrounding bones with implants.

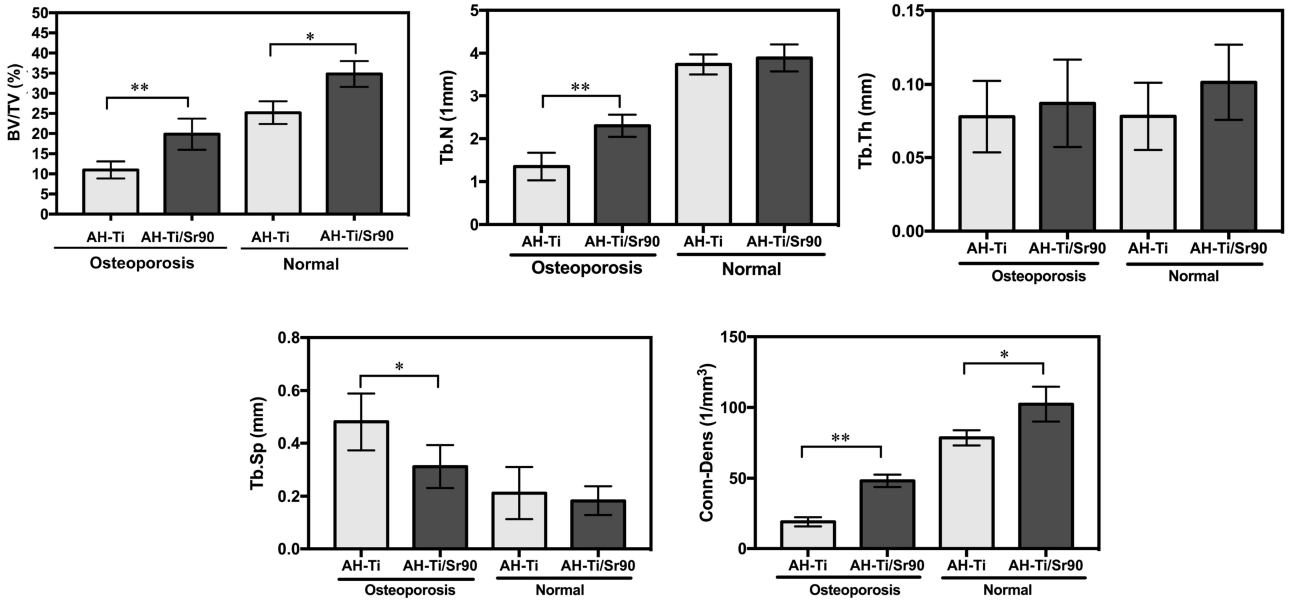

Figure 9 Corresponding quantitative analysis results of BV/TV, Tb.N, Tb.Th, Tb.Sp and Conn-Dens. *P<0.05, **P<0.01.

nuclear and thus enhanced the nuclear transcription.[61] As for osteoclast inhibition, strontium could decrease the expression of rank ligand and increased the expression of *OPN* and thus inhibit the pro-osteoclast's differentiation.-[61,62] Combined with the in vitro experiments, we speculated that the two-way regulation (osteogenic induction and osteoclast inhibition) accounts for the AH-Ti/Sr90 induced promotion in the osteoporotic model than in the normal rat model.

Li et al had compared the four different surface implants (smooth-structure, microstructure, nanostructure and micro/nanostructure)in in vivo experiment, and found that the microstructure and micro/nanostructure showed the best osteointegration.[37] However, the nanostructure modified on

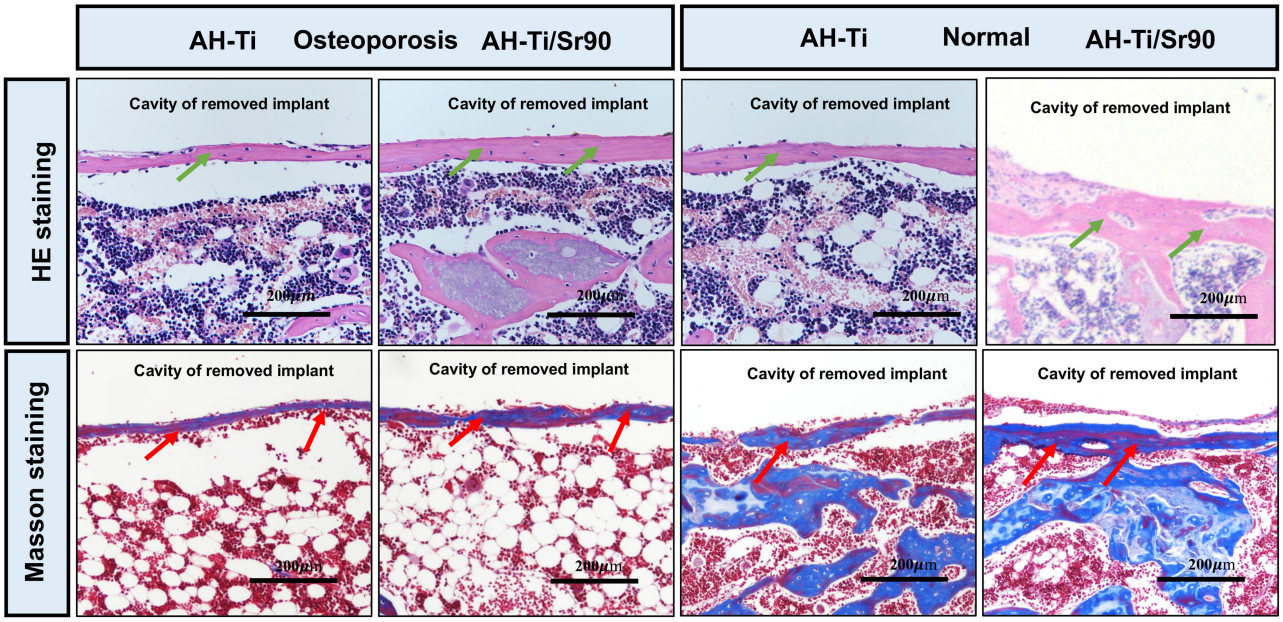

Figure 10 Histological analysis of new bone formation around the implants.

titanium had been proved inadequate to enhance the osteointegration in vivo by previous study.[63] Therefore, we could conclude that the strontium plays a pivotal role in osteointegration promotion.

Histological Analysis

The H&E staining and Masson staining were applied to detect the new bone formation around the implant. As shown in Figure 10 the trabecular bone represented by the red zone stained by H&E stain in the AH-Ti/Sr90 group showed increased thickness compared to the control group both in normal and osteoporotic rat models. In addition, the staining results showed that there were more osteoid tissues around the AH-Ti/Sr90 group than in the control group. In the Masson staining samples, the new bone shown by blue tissue, which represented immature trabecular bone was obviously thicker in AH-Ti/Sr90 than in AH-Ti groups both in osteoporotic and normal models. What is more, the newly formed bone in AH-Ti/Sr90 seemed consequent while it was intermittent in AH-Ti group. The results indicated that the newly formed bone in the AH-Ti/Sr90 group could grow from the parent bone to marrow cavity and formed along the bone-to-implant interface and thus promoted osteointegration, which was in agreement with the micro-CT evaluation. Therefore, the in vivo experiments indicated that the modification of the 90 min $SrTiO_3$ nanocoating could enhance new bone formation and promote the osteointegration tremendously both in osteoporotic and normal models. In addition, the osteoclast inhibition of strontium function made the AH-Ti/Sr90 implant more effective in osteoporotic rats.

Conclusion

The AH-Ti/Sr surface was successfully fabricated by hot-alkaline treatment and magnetron sputtering. Strontium nanocoating modified the surface topography, increased the surface roughness and hydrophilicity, and altered the surface element component. We found that AH-Ti/Sr90 possessed best cytocompatibility including cell morphology, cell viability and cell differentiation due to the suitable and long-lasting strontium ion release. In addition, AH-Ti/Sr90 could enhance the osteogenic related gene expressions and inhibit the osteoclast genes (*RANKL* and *TRAP*) thus enhancing osteogenic differentiation and inhibiting the bone resorption. Moreover, the AH-Ti/Sr90 significantly promoted the osteointegration both in normal and osteoporotic rat models. Therefore, we can conclude that the AH-Ti/Sr90 is a promising implant system and can provide a novel idea for implant research, of which the drug loading studies will be applied for further optimization.

Funding

This work was financially supported by Wenzhou Municipal Science and Technology Project for Public Welfare (Y20190498 and Y2020120).

Disclosure

The authors report no conflicts of interest in this work.

References

1. Geetha M, Singh AK, Asokamani R, et al. Ti based biomaterials, the ultimate choice for orthopaedic implants - A review. *Prog Mater Sci*. 2009;54(3):397–425. doi:10.1016/j.pmatsci.2008.06.004
2. Wu S, Liu X, Yeung KWK, et al. Surface nano-architectures and their effects on the mechanical properties and corrosion behavior of Ti-based orthopedic implants. *Surf Coat Tech*. 2013;233:13–26. doi:10.1016/j.surfcoat.2012.10.023
3. Iii C, Charles H. Osteoporosis, an Underdiagnosed Disease. *JAMA*. 2001;286(22):2865. doi:10.1001/jama.286.22.2865
4. Mathilde G, Genevive P, et al. Functionalization of titanium implant surface for improving osteointegration. *Front Bioeng Biotech*. 2016;4.
5. Asokamani R. Bacterial and mammalian cells adhesion to tantalum-decorated micro-/nano-structured titanium. *J Biomed Mater Res*. 2017;105(3). doi:10.1002/jbm.a.35953
6. Yuan B, Cheng Q, Zhao R, et al. Comparison of osteointegration property between PEKK and PEEK: effects of surface structure and chemistry. *BIOMATERIALS*. 2018:S0142961218302606. doi:10.1016/j.biomaterials.2018.04.014
7. Jimbo R, Anchieta R, Baldassarri M, et al. Histomorphometry and bone mechanical property evolution around different implant systems at early healing stages: an experimental study in dogs. *Implant Dent*. 2013;22(6):6. doi:10.1097/ID.0b013e31829f1f4b
8. Ang G, et al. The effects of titania nanotubes with embedded silver oxide nanoparticles on bacteria and osteoblasts. *Biomaterials*. 2014. doi:10.1016/j.biomaterials.2014.01.058
9. Zhang K, Zhu Y, Liu X, et al. Sr/ZnO doped titania nanotube array: an effective surface system with excellent osteoinductivity and self-antibacterial activity. *Mater Design*. 2017;130:403–412. doi:10.1016/j.matdes.2017.05.085
10. Sedira S, Achour S, Avci A, et al. Physical deposition of carbon doped titanium nitride film by DC magnetron sputtering for metallic implant coating use. *APPL SURF SC*. 2014;295:81–85. doi:10.1016/j.apsusc.2014.01.010
11. K G N, Puleo DA. Effect of metal ions on the formation and function of osteoclastic cells in vitro. *J Biomed Mater Res A*. 1997;35(2):265–271. doi:10.1002/(SICI)1097-4636(199705)35:23.0.CO;2-G
12. Morra M, Cassinelli C, Cascardo G, et al. Surface engineering of titanium by collagen immobilization. Surface characterization and in vitro and in vivo studies. *Biomaterials*. 2003;24(25):4639–4654. doi:10.1016/s0142-9612(03)00360-0
13. Lu T, Wen J, Qian S, et al. Enhanced osteointegration on tantalum-implanted polyetheretherketone surface with bone-like elastic modulus. *Biomaterials*. 2015;51:173–183. doi:10.1016/j.biomaterials.2015.02.018
14. V V D R, Vinoth-Kumar L, V C A, et al. Osteointegration of titanium implant is sensitive to specific nanostructure morphology. *Acta Biomater*. 2012;8(5):1976–1989. doi:10.1016/j.actbio.2012.01.021
15. R K S, P G F, Sjöström T, et al. Analysis of Osteoclastogenesis/Osteoblastogenesis on Nanotopographical Titania Surfaces. *Adv Healthc Mater*. 2016;5(8):947–955. doi:10.1002/adhm.201500664
16. Teixeira S, Monteiro FJ, Ferraz MP, et al. Laser surface treatment of hydroxyapatite for enhanced tissue integration: surface characterization and osteoblastic interaction studies. *J Biomed Mater Res A*. 2010;81A(4:920–929. doi:10.1002/jbm.a.31073
17. Liu R, Ma Z, S K K, et al. In vitro study on cytocompatibility and osteogenesis ability of Ti–Cu alloy. *J Mater Sci Mater Med*. 2019;30(7):75. doi:10.1007/s10856-019-6277-z
18. Rajendran A, Deepak K. Pattanayak. Silver incorporated antibacterial, cell compatible and bioactive titania layer on Ti metal for biomedical applications. *RSC Adv*. 2014;4(106):61444–61455. doi:10.1039/C4RA13107J
19. Cochis A, Azzimonti B, Della Valle C, et al. The effect of silver or gallium doped titanium against the multidrug resistant Acinetobacter baumannii. *BIOMATERIALS*. 2016;80:80–95. doi:10.1016/j.biomaterials.2015.11.042
20. J W P, Y J K, J H J, et al. Surface characteristics and primary bone marrow stromal cell response of a nanostructured strontium-containing oxide layer produced on a microrough titanium surface. *J Biomed Mater Res A*. 2012;100A(6:1477–1487. doi:10.1002/jbm.a.34085
21. Chandran S, Shenoy SJ, Babu SS, et al. Strontium Hydroxyapatite scaffolds engineered with stem cells aid osteointegration and osteogenesis in osteoporotic sheep model. *Colloids Surf B Biointerfaces*. 2014:S0927776517308883. doi:10.1016/j.colsurfb.2017.12.048
22. Braux J, Velard F, Guillaume C, et al. A new insight into the dissociating effect of strontium on bone resorption and formation. *Acta Biomater*. 2011;7(6):2593–2603. doi:10.1016/j.actbio.2011.02.013
23. Bonnelye E, Chabadel A, Saltel F, et al. Dual effect of strontium ranelate: stimulation of osteoblast differentiation and inhibition of osteoclast formation and resorption in vitro. *BONE*. 2008;42(1):129–138. doi:10.1016/j.bone.2007.08.043
24. Bianchi M, Degli Esposti L, Ballardini A, et al. Strontium doped calcium phosphate coatings on poly (etheretherketone) (PEEK) by pulsed electron deposition. *SURF COAT TECH*. 2017;319:191–199. doi:10.1016/j.surfcoat.2017.04.012
25. Wang G, Wan Y, Ren B, et al. Surface functionalization of micro/nanostructured titanium with bioactive ions to regulate the behaviors of murine osteoblasts. *Adv Eng Mater*. 2017;19(11):1700299. doi:10.1002/adem.201700299
26. Capuccini C, Torricelli P, Sima F, et al. Strontium-substituted hydroxyapatite coatings synthesized by pulsed-laser deposition: in vitro osteoblast and osteoclast response. *Acta Biomater*. 2008;4(6):1885–1893. doi:10.1016/j.actbio.2008.05.005
27. Zhao L, Wang H, Huo K, et al. The osteogenic activity of strontium loaded titania nanotube arrays on titanium substrates. *BIOMATERIALS*. 2013;34(1):19–29. doi:10.1016/j.biomaterials.2012.09.041
28. Ding X, Wang Y, Xu L, et al. Stability and osteogenic potential evaluation of micro-patterned titania mesoporous-nanotube structures. *INT J NANOMED*. 2019;14:4133. doi:10.2147/IJN.S199610
29. Yu Y, Shen X, Luo Z, et al. Osteogenesis potential of different titania nanotubes in oxidative stress microenvironment. *BIOMATERIALS*. 2018;167:44. doi:10.1016/j.biomaterials.2018.03.024
30. Wang T, Wan Y, Liu Z. Fabrication of hierarchical micro/nanotopography on bio-titanium alloy surface for cytocompatibility improvement. *J MATER SCI*. 2016;51(21):9551–9561. doi:10.1007/s10853-016-0219-7
31. Zhou Y, Y B W, E W Z, et al. Alkali-heat treatment of a low modulus biomedical Ti–27Nb alloy. *Biomed Mater*. 2009;4(4):044108. doi:10.1088/1748-6041/4/4/044108
32. R A G, Scheideler L, Rupp F, et al. A review on the wettability of dental implant surfaces II: biological and clinical aspects. *Acta Biomater*. 2014;10(7):2907–2918. doi:10.1016/j.actbio.2014.03.032
33. Vlacic-Zischke J, S M H, Friis T, et al. The influence of surface microroughness and hydrophilicity of titanium on the up-regulation of TGFβ/BMP signalling in osteoblasts. *BIOMATERIALS*. 2011;32(3):665–671. doi:10.1016/j.biomaterials.2010.09.025
34. Yamamura K, Miura T, Kou I, et al. Influence of various super hydrophilic treatments of titanium on the initial attachment, proliferation, and differentiation of osteoblast-like cells. *Dent Mater J*. 2015:2014–2076. doi:10.4012/dmj.2014-076
35. Pandey P, Roy S. Is it possible to change wettability of hydrophilic surface by changing its roughness? *J Phys Chem Lett*. 2013;4(21):3692–3697. doi:10.1021/jz401946v
36. Puckett SD, Webster TJ, Raimondo T, Webster TJ. The relationship between the nanostructure of titanium surfaces and bacterial attachment. *BIOMATERIALS*. 2010;31(4):706–713. doi:10.1016/j.biomaterials.2009.09.081
37. Li Y, Qi Y, Gao Q, et al. Effects of a micro/nano rough strontium-loaded surface on osseointegration. *INT J NANOMED*. 2015;10:4549. doi:10.2147/IJN.S84398
38. Lu L, Wu L, Chen J, et al. Effects of sodium on rat osteoblast and the role of epithelial sodium channel. *Nan Fang Yi Ke Da Xue Xue Bao*. 2011;31(11):1871–1874. doi:10.1038/cmi.2011.4

39. Wang Y, Zhang D, Wen C, Li Y. Processing and Characterization of SrTiO 3 –TiO Nanoparticle–Nanotube Heterostructures on Titanium for Biomedical Applications. *ACS Appl Mater Interfaces*. 2015;7(29):16018–16026. doi:10.1021/acsami.5b04304
40. McBeath R, D M P, C M N, et al. Cell shape, cytoskeletal tension, and RhoA regulate stem cell lineage commitment. *Dev Cell*. 2004;6(4):483–495. doi:10.1016/s1534-5807(04)00075-9
41. Mine Y, Makihira S, Nikawa H, et al. Impact of titanium ions on osteoblast-, osteoclast- and gingival epithelial-like cells. *J Prosthodont Res*. 2010;54(1):1–6. doi:10.1016/j.jpor.2009.07.003
42. Hahn A, Fuhlrott J, Loos A, et al. Cytotoxicity and ion release of alloy nanoparticles. *J Nanopart Res*. 2012;14(1):1–10. doi:10.1007/s11051-011-0686-3
43. Gholinejad Z, Khadem Ansari MH, Rasmi Y. Titanium dioxide nanoparticles induce endothelial cell apoptosis via cell membrane oxidative damage and p38, PI3K/Akt, NF-κB signaling pathways modulation. *J TRACE ELEM MED BIO*. 2019;54:27–35. doi:10.1016/j.jtemb.2019.03.008
44. Hallab NJ, Skipor A, Jacobs JJ. Interfacial kinetics of titanium- and cobalt- based implant alloys in human serum: metal release and biofilm formation. *J Biomed Mater Res A*. 2003;65(3):311–318. doi:10.1002/jbm.a.10429
45. Capuccini C, Torricelli P, Sima F, et al. Strontium-substituted hydroxyapatite coatings synthesized by pulsed-laser deposition: in vitro osteoblast and osteoclast response. *Acta Biomater*. 2008;4(6):1885–1893. doi:10.1016/j.actbio.2008.05.005
46. J W P, H K K, Y J K, et al. Osteoblast response and osseointegration of a Ti–6Al–4V alloy implant incorporating strontium. *Acta Biomater*. 2010;6(7):2843–2851. doi:10.1016/j.actbio.2010.01.017
47. A S H-L, Mentaverri R, Caudrillier A, et al. The calcium-sensing receptor is involved in strontium ranelate-induced osteoclast apoptosis new insights into the associated signaling pathways. *J Biol Chem*. 2009;284(1):575–584. doi:10.1074/jbc.M801668200
48. Roy M, Bose S. Osteoclastogenesis and osteoclastic resorption of tricalcium phosphate: effect of strontium and magnesium doping. *J Biomed Mater Res A*. 2012;100(9):2450–2461. doi:10.1002/jbm.a.34181
49. Sone E, Noshiro D, Ikebuchi Y, et al. The induction of RANKL molecule clustering could stimulate early osteoblast differentiation. *BIOCHEM BIOPH RES CO*. 2019;509(2):435–440. doi:10.1016/j.bbrc.2018.12.093
50. K A K, Bugarija B, B T L, et al. Geometric cues for directing the differentiation of mesenchymal stem cells. *P NATL ACAD SCI*. 2010;107(11):4872–4877. doi:10.1073/pnas.0903269107
51. Lin Z, Zhao X, Chen S, et al. Osteogenic and tenogenic induction of hBMSCs by an integrated nanofibrous scaffold with chemical and structural mimicry of the bone–ligament connection. *J MATER CHEM B*. 2017;5(5):1015–1027. doi:10.1039/C6TB02156E
52. Yao L, Wu X, Wu S, et al. Atomic layer deposition of zinc oxide on microrough zirconia to enhance osteogenesis and antibiosis. *CERAM INT*. 2019;45(18):24757–24767. doi:10.1016/j.ceramint.2019.08.216
53. Anselme K. Osteoblast adhesion on biomaterials. *BIOMATERIALS*. 2000;21(7):667–681. doi:10.1016/s0142-9612(99)00242-2
54. Zhang W, Wang G, Liu Y, et al. The synergistic effect of hierarchical micro/nano-topography and bioactive ions for enhanced osseointegration. *BIOMATERIALS*. 2013;34(13):3184–3195. doi:10.1016/j.biomaterials.2013.01.008
55. Zhao L, Mei S, P K C, et al. The influence of hierarchical hybrid micro/nano-textured titanium surface with titania nanotubes on osteoblast functions. *BIOMATERIALS*. 2010;31(19):5072–5082. doi:10.1016/j.biomaterials.2010.03.014
56. Gao A, Liao Q, Xie L, et al. Tuning the surface immunomodulatory functions of polyetheretherketone for enhanced osseointegration. *BIOMATERIALS*. 2020;230:119642. doi:10.1016/j.biomaterials.2019.119642
57. Jin G, Qin H, Cao H, et al. Synergistic effects of dual zn/ag ion implantation in osteogenic activity and antibacterial ability of titanium. *BIOMATERIALS*. 2014;35(27):7699–7713. doi:10.1016/j.biomaterials.2014.05.074
58. Yi T, Zi-Min W, Jun-Ling C, et al. Reconstruction of radial head with autogenous iliac bone enhance stability of elbow joint: animal experimental study. *Chin J Bone Joint Injury*. 2017;2:1254.
59. Pi M, Quarles LD, et al. A novel cation-sensing mechanism in osteoblasts is a molecular target for strontium. *J Bone Mineral Res*. 2010;19:5.
60. Almeida MM, Nani EP, Teixeira LN, et al. Strontium ranelate increases osteoblast activity. *Tissue Cell*. 2016;48(3):183–188. doi:10.1016/j.tice.2016.03.009
61. Yang F, Yang D, Tu J, et al. Strontium enhances osteogenic differentiation of mesenchymal stem cells and in vivo bone formation by activating wnt/catenin signaling. *Stem Cells*. 2011;29(6):981–991. doi:10.1002/stem.646
62. Suzuki G, Hirota M, Hoshi N, et al. Effect of Surface Treatment of Multi-Directionally Forged (MDF) Titanium Implant on Bone Response. *METALS*. 2019;9(2):23. doi:10.3390/met9020230
63. Meirelles L, Arvidsson A, Albrektsson T, et al. Increased bone formation to unstable nano rough titanium implants. *CLIN ORAL IMPLAN RES*. 2007;18(3):326–332. doi:10.1111/j.1600-0501.2006.01308.x